Enhanced all-optical switching with double slow light pulses

Chi-Ching Lin,[1] Meng-Chang Wu,[1] Bor-Wen Shiau,[1] Yi-Hsin Chen,[2] Ite A. Yu,[2] Yong-Fan Chen,[3] and Ying-Cheng Chen[1,2,*]

[1]*Institute of Atomic and Molecular Sciences, Academia Sinica, Taipei 10617, Taiwan*

[2]*Department of Physics and Frontier Research Center on Fundamental and Applied Sciences of Matters, National Tsing Hua University, Hsinchu 30013, Taiwan*

[3]*Department of Physics, National Cheng Kung University, Tainan 70101, Taiwan*

(Received 14 March 2012; revised manuscript received 8 August 2012; published 28 December 2012)

We experimentally demonstrate an all-optical switching (AOS) scheme based on double slow light (DSL) pulses, in which one pulse is switched by another due to the cross-Kerr nonlinearity. The interaction time is prolonged by optically dense atomic media and matched group velocities. The interaction strength is maintained at a high level by keeping both fields at their electromagnetically-induced-transparency resonances to minimize the linear loss. In the AOS without the DSL scheme, the group velocity mismatch sets an upper limit on the switching efficiency of two photons per atomic cross section as discussed by Harris and Hau [Phys. Rev. Lett. **82**, 4611 (1999)]. Compared to that limit, we have obtained an enhanced switching efficiency by a factor of 3 with our DSL scheme. The nonlinear efficiency can be further improved by increasing the optical depth of the medium. Our work advances low-light-level nonlinear optics and provides essential ingredients for quantum many-body physics using strongly interacting photons.

DOI: 10.1103/PhysRevA.86.063836 PACS number(s): 42.50.Gy, 32.80.Qk, 42.65.Hw

I. INTRODUCTION

Photons are ideal carriers of quantum information due to their high propagation speed and weak coupling nature. However, a strong nonlinear interaction between photons is crucial in many quantum information processing applications. Atomic medium in the presence of electromagnetically induced transparency (EIT) [1] provides an avenue to obtaining strong nonlinear photon-photon interactions. The four-level N-type system is a basic EIT-based scheme for the implementation of nonlinear optical processes, such as all-optical switching, cross-phase modulation, and four-wave mixing [2–4]. It has been predicted to allow nonlinear optical processes at energies per area of a few photons per atomic cross section [3,4]. In the N-type system, the probe pulse is a slow light but the switching pulse propagates at the vacuum speed of light. This group velocity mismatch sets an upper limit to the interaction time and thus the nonlinear efficiency. To overcome this limitation, the double slow light (DSL) scheme has been proposed [5–9]. In the DSL scheme the nonlinear efficiency is determined by the group delay time, which in principle has no upper limit but only depends on the achievable optical depth (OD).

Previously, we have demonstrated a DSL scheme in cold cesium atoms [10]. The cross-Kerr nonlinearity is obtained through two five-level asymmetric M-type systems [11,12]. Although we have implemented the DSL scheme in that study, the performance of the cross-phase modulation did not overcome the N-type limit [10]. The reason is the accompanying linear loss in the switching EIT system, in which a two-photon detuning is introduced to induce the cross-Kerr nonlinearity. The gain in the interaction time is canceled by the loss in the interaction strength. We here demonstrate an improved DSL scheme that allows for a nonzero cross-Kerr nonlinearity but with both weak fields kept at their EIT resonances. This scheme takes the full advantage of the DSL. We study the nonlinear process of all-optical switching (AOS), controlling the attenuation of probe pulses by switching pulses, which is related to the imaginary part of the cross-Kerr susceptibility [13,14]. In the N-type scheme with both pulses firing at the same time, a maximum switching efficiency of two photons per atomic cross section is needed to induce an attenuation of the probe to e^{-1} [13]. With our scheme, we obtain a significant enhancement of the AOS efficiency over that obtained with our previous DSL scheme [10]. In addition, it allows us to overcome the N-type switching limit by a factor of 3. If this DSL scheme can be combined with tightly transverse confinement [15], it will offer the opportunity to realize single-photon-level optical devices [3,4,11], as well as the intriguing quantum many-body physics utilizing strongly interacting photons [16–18].

A schematic diagram of our DSL and AOS scheme is shown in Fig. 1(a). The population is prepared in states $|1\rangle$ and $|6\rangle$ by the optical pumping method. The probe and control 1 (switching and control 2) form a Λ-type EIT for the states $|1\rangle$ to $|3\rangle$($|6\rangle$ to $|8\rangle$). The five states $|1\rangle$ to $|5\rangle$ and the other five $|6\rangle$ to $|10\rangle$ form two sets of asymmetric M-type systems (denoted by M_1 and M_2) as shown in Figs. 1(b) and 1(c) [11,12]. In our improved AOS scheme, we apply a small magnetic field in the laser propagation direction to lift the Zeeman degeneracy. We keep all laser fields on their one-photon resonances with respect to the right Λ section in the two M-type systems. Therefore, both EIT systems are on their two-photon resonances. However, the left Λ sections are two-photon detuned due to the difference in Zeeman shifts. Thus the cross-Kerr susceptibilities are nonzero even with both EIT systems on their two-photon resonances.

II. THEORETICAL ANALYSIS

Before discussing the experiment, we first consider a theoretical analysis of the AOS based on the DSL scheme to grasp essential idea. Under the slowly varying envelope approximation and considering to the first-order dispersion, the Maxwell

*chenyc@pub.iams.sinica.edu.tw

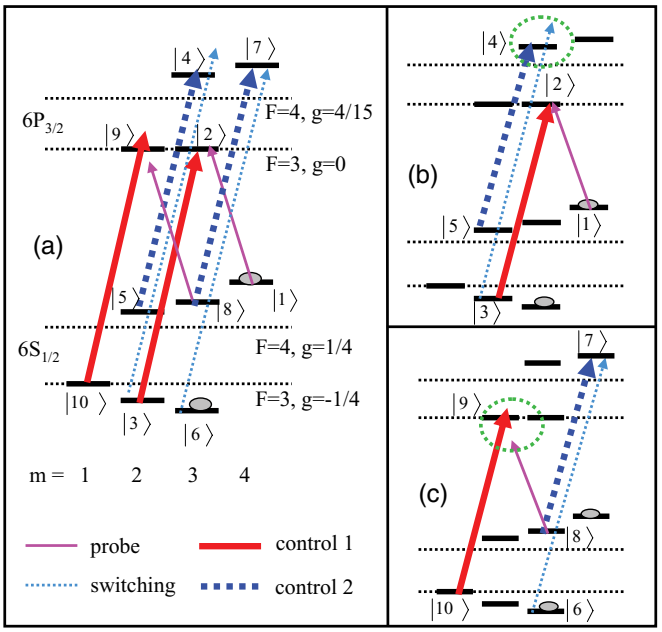

FIG. 1. (Color online) (a) Relevant energy levels for ^{133}Cs atoms and laser excitations in the presence of a magnetic field. (b), (c) The M-type five-level systems formed by states $|1\rangle$ to $|5\rangle$ (M_1) and $|6\rangle$ to $|10\rangle$ (M_2).

equations for the probe and switching fields are [19,20],

$$\frac{\partial \Omega_{p(s)}}{\partial z} + \frac{1}{v_g^{p(s)}} \frac{\partial \Omega_{p(s)}}{\partial t} = i \frac{k_{p(s)}}{2} \chi_{p(s)} \Omega_{p(s)}, \tag{1}$$

where $\Omega_{p(s)} = -\frac{\mu_{12(67)} E_{p(s)}}{\hbar}$, $k_{p(s)}$, $v_g^{p(s)}$, and $\chi_{p(s)}$ are the Rabi frequency, wave vector, group velocity, and susceptibility of the probe (switching) field, respectively. The susceptibility is proportional to the density matrix element that can be obtained by solving the optical Bloch equation (OBE) [10]. Because the energy level scheme is relatively complicated, we consider the following simplifications in the probe and switching susceptibilities to capture the major physics. We have performed a numerical calculation of the OBE for the ten-level system shown in Fig. 1(a). Both the steady-state and transient calculations have been performed. From the calculation, we find that the overall atomic responses from ρ_{21} and ρ_{98} resemble the results from a simple five-level system like the M_1 only. The difference in the cross-Kerr susceptibility of probe ($\chi_p^{(3,ck)}$) for the actual ten-level system to the simplified five-level M_1 system is less than 15% with the typical experimental parameters. Thus, $\chi_p^{(3,ck)} \simeq \chi_{p,M_1}^{(3,ck)}$. Detailed analysis and explanation to support this point are shown in the Appendix. In the experiment, we are only concerned with the nonlinear loss of the probe due to the switching. The linear and self-Kerr susceptibilities for the probe are not considered. In addition, we consider the cases with $\Omega_p \ll \Omega_s$ such that only the nonlinear loss of the probe due to the switching needs to be considered but not the opposite. Under such an assumption, the cross-Kerr contributions to χ_s is negligible and χ_s can be approximated by the linear susceptibility, $\chi_{s,M_2}^{(1)}$. The analytic form of $\chi_{p,M_1}^{(3,ck)}$ and $\chi_{s,M_2}^{(1)}$ can be derived using perturbation theory and are shown below [10,12],

$$\chi_{p,M1}^{(3,ck)} = \frac{n_p \sigma_p}{2k_p} \frac{-i(i\delta_4 - \gamma)\Gamma/4}{\left[(i\delta_p - (\Gamma+\gamma)/2)(i\delta_2 - \gamma) + \Omega_{c1}^2/4\right]\left[(i\delta_3 - (\Gamma+\gamma)/2)(i\delta_4 - \gamma) + \Omega_{c2}^2/4\right]}, \tag{2}$$

and

$$\chi_{s,M_2}^{(1)} = \frac{n_s \sigma_s}{2k_s} \frac{-i(i(\delta_s - \delta_{c2}) - \gamma)\Gamma}{[i\delta_s - (\Gamma+\gamma)/2][i(\delta_s - \delta_{c2}) - \gamma] + \Omega_{c2}^2/4}. \tag{3}$$

The notations $n_{p(s)}, \sigma_{p(s)}, \Gamma, \gamma$ indicate the atomic density in state $|1\rangle$ ($|6\rangle$), the absorption cross section for the probe (switching) transition, the excited state decay rate and the ground-state decoherence rate, respectively. $\delta_{p(s)}$ is the probe (switching) detuning and the multiphoton detunings are $\delta_2 = \delta_p - \delta_{c1}, \delta_3 = \delta_2 + \delta_s, \delta_4 = \delta_3 - \delta_{c2}$.

Considering a coordinate transformation that copropagates with the switching pulse, the Maxwell equation for the switching field can be solved to be [20], $\Omega_s(z,t) = \Omega_s(0, t - \frac{z}{v_g^s}) \exp(\frac{i}{2} k_s \chi_s^{(1)} z)$. Inserting this result into Eq. (1) and considering similar transformation for the probe pulse, assuming $v_g^p = v_g^s$ and considering the cross-Kerr effect only, the probe solution is [12,19],

$$\frac{\Omega_p(z,t)}{\Omega_p(0,\tau)} = \exp\left[\frac{i}{2} k_p \int_0^z dz' \chi_p^{(3,ck)} |\Omega_s(0,\tau)|^2 e^{-k_s Im(\chi_s^{(1)} z')}\right], \tag{4}$$

where $\tau = t - \frac{z}{v_g^p}$. Thus the intensity transmission for a square probe pulse due to the nonlinear loss is,

$$T_p = \exp\left\{-\frac{k_p \mathrm{Im}(\chi_p^{(3,ck)}) |\Omega_{s0}|^2}{k_s \mathrm{Im}(\chi_s^{(1)})} \left[1 - \exp\left(-k_s \mathrm{Im}(\chi_s^{(1)}) L\right)\right]\right\}, \tag{5}$$

where L is the sample length. From Eqs. (4) and (5), one observes that when $\mathrm{Im}(\chi_s^{(1)})$ is minimized (i.e., the switching field is at its EIT resonance) the nonlinear switching on the probe is maximized. This fact highlights the main point of our DSL scheme.

From the definitions of the Rabi frequency, we note that $\Omega_{s0}^2 \tau_s = \frac{N_s \sigma_s \Gamma}{A}$ for square pulses, where τ_s, N_s, σ_s, and A are the duration of the switching pulse, number of switching photons, absorption cross section for switching transition, and the laser cross section, respectively. Eq. (5) can be written as,

$$T_p = \exp\left(-\psi \frac{N_s}{A} \sigma_s\right), \tag{6}$$

where ψ is a parameter characterizing the nonlinear switching efficiency. This form also holds for different pulse waveforms and schemes but with different ψ. Next, we consider the

Gaussian waveform for both pulses. The maximum efficiency ψ at the probe peak for the N-type system is [4]

$$\psi = \frac{1}{2}\mathrm{erf}\left(\frac{\sqrt{4ln2}\alpha_p\Gamma}{\tau_s\Omega_{c1}^2}\right), \tag{7}$$

where τ_s is the intensity FWHM duration of the switching pulse and α_p is the OD for the probe. In the DSL scheme, we tune the magnetic field to a value such that $\chi_p^{(3,ck)}$ is operated under maximum switching conditions. With $\delta_p = 0$ and $\delta_2 = 0$, it can be shown from Eq. (2) that the maximum switching condition occurs when the two-photon detuning for the left Λ section in the M_1 system is equal to $\Omega_{c2}/2$ with respect to the $|5\rangle \rightarrow |4\rangle$ transition. The maximum value of $k_p\mathrm{Im}(-\chi_{p,M1}^{(3,ck)})$ is $\frac{n_s\sigma_s}{\Omega_{c1}^2}$ if $\gamma \ll \Gamma$. From Eq. (3), it can be shown that the minimum value of $k_s\mathrm{Im}(\chi_s^{(1)})$ is $n_s\sigma_s\frac{2\Gamma\gamma}{\Omega_{c2}^2}$. If we maintain $v_g^{(p)} = v_g^{(s)}$ and $\alpha_p = \alpha_s$, then $\Omega_{c1} = \Omega_{c2}$ since the group delay $T_D = \frac{\alpha\Gamma}{\Omega_c^2}$. Inserting all these relations into Eq. (4), the efficiency ψ for the DSL scheme is,

$$\psi = \frac{1}{\tau_s}\sqrt{\frac{4ln2}{\pi}}\frac{1-\exp\left(-2\gamma\frac{\alpha_s\Gamma}{\Omega_{c2}^2}\right)}{2\gamma}. \tag{8}$$

It is evident that ψ is proportional to α_s at low α_s and is saturated to a value determined by γ at high α_s.

However, this estimation of ψ is too optimistic if one considers to the second-order dispersion, which causes pulse broadening and reduction in amplitude and thus a degradation of ψ [10,21]. Considering to the second-order dispersion, the intensity temporal width for a pulse passing through an EIT medium is broadened by a factor of $\beta = \sqrt{1+16\ln 2\alpha\Gamma^2/\tau^2\Omega_c^4}$ and the peak intensity is reduced by a factor of $1/\beta^2$ [10,21]. If we include this effect for the switching into Eq. (4), the efficiency ψ is,

$$\psi = \frac{n_p\sigma_p\Gamma}{\tau_s\Omega_{c1}^2}\sqrt{\frac{4\ln 2}{\pi}}\int_0^L \frac{\exp\left(-\frac{2\gamma\Gamma}{\Omega_{c2}^2}n_s\sigma_s z\right)}{1+\frac{16\ln 2\Gamma^2}{\tau_s^2\Omega_{c2}^4}n_s\sigma_s z}dz. \tag{9}$$

The broadening effect on the probe pulse is not considered because it will be normalized away. Based on Eq. (9), one can show that at a fixed OD there is an optimum Ω_c that maximizes ψ. With higher ODs, both the optimum Ω_c and maximum ψ shift to higher values. The square of the optimum Ω_c and the maximum ψ scale with $\sqrt{\alpha_p}$ [5,22].

III. EXPERIMENTAL SETUP

Our experiment was performed with a two-dimensional magneto-optical trap (MOT) [23]. We typically trap $(1–3)\times 10^9$ atoms with a total trapping power of 240 mW and a repumping power of 25 mW. The length of the atomic cloud is $\sim$2 cm. We use a combination of techniques to increase the ODs including the temporal dark MOT and optical pumping. Before turning off the quadruple magnetic field of the MOT for performing the measurements, the intensity of the repumping beam of MOT is reduced by a factor of $\sim$30 for 4 ms to increase the atom density. The optical pumping is performed by applying both control fields for 0.5 ms before the measurements. In the cases that we need to adjust the population ratio among the state $|1\rangle$ and $|6\rangle$, we apply one additional optical pumping beam with a frequency of 3 MHz red-detuned to the $|F=3\rangle \rightarrow |F'=4\rangle$ σ^+−transition. The OD ratio among the probe and switching transitions can be adjust by varying the intensity of this laser beam. Typical ODs for the probe and switching transitions are around 50–100.

One master laser is frequency-stabilized to the cesium absorption line. It injection locks one slave laser and one vertical-cavity surface-emitting laser (VCSEL), which is current modulated around 9 GHz. The VCSEL injection locks another slave laser at its +1 sideband. Thus, the two slave lasers maintain a good mutual coherence with a frequency offset of about the ground-state hyperfine splitting of cesium. The control, switching, and probe beams are all derived from the two slave lasers. Some acousto-optic modulators (AOMs) are used to generate the laser fields at desired frequencies. The probe and switching beams are combined through a polarizing beam splitter. They are coupled into a polarization-maintaining fiber to ensure perfect overlapping for good AOS. The probe and switching beams are converted to circular polarizations by a quarter wave plate. They are focused to a waist of 50 μm within the atomic cloud with a Rayleigh length of $\sim$1 cm. The control beams are coupled with the probe and switching beams through two beam splitters. All laser beams propagate along the long axis of the atom clouds. The diameters of the control beams are $\sim$4 mm to cover the atomic cloud. The control beams intersect with the probe and switching beams by $\sim 1^0$. After the MOT, the probe and switching beams pass through another quarter wave plate to be converted into linear polarizations. They are split by a polarizing beam splitter and then detected by two photomultiplier tubes (PMTs, Hamamatsu H6780-20) with an overall efficiency of 40% and 28% for the probe and switching, respectively. A series of irises, pinholes, and multimode fibers are used to minimize the leakage of the strong control beams into the PMTs with overall extinction ratios of better than 70 dB.

The stray magnetic field is compensated by three pairs of coils to less than 3 mG. Some electronics are used to quickly damp the current through the MOT coils within 0.5 ms. We avoid placing metallic components near the MOT region in order to minimize the inhomogeneous magnetic field produced by the induced eddy current. With such arrangements, the ground-state decoherence rate is kept to 1×10^{-3} Γ level, which is determined from the EIT spectral fitting. In our DSL scheme, we have to apply a magnetic field of a few Gauss along the long axis of the atom clouds. We apply a pulsed magnetic field with a duration of 2 ms during the MOT off period to minimize the perturbation on the MOT. A capacitor in addition with one power supply are used to apply the current through one pair of compensation magnetic coils with an e^{-1} time constant of $\sim$0.2 ms. The MOT is off for 1.5 ms for the AOS experiment at a 50-Hz repetition rate. We apply two subsequent probe pulses and one switching pulse in coincident with the second probe pulse. The power ratio of the second to the first probe pulse reflects the nonlinear loss due to the switching pulse.

IV. RESULTS AND DISCUSSIONS

We first measure the transmission spectrum of the probe versus the detuning of the switching field (δ_s) without a

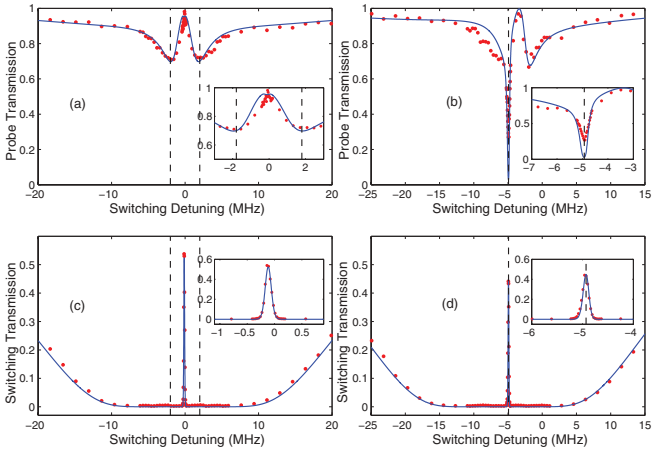

FIG. 2. (Color online) (a), (b) T_p versus δ_s. (c), (d) Switching transmission versus δ_s. (a) and (c) [(b) and (d)] were taken without (with) the presence of a (1.9 G) magnetic field. The δ_s here are laser detunings with respect to the magnetic-field-free resonant frequency of transition $|6\rangle \rightarrow |7\rangle$. The blue traces in (a) and (b) [(c) and (d)] indicate the theoretical curves obtained using Eq. (5) (EIT line shape). The parameters $\{\alpha_p,\alpha_s,\Omega_{c1},\Omega_{c2},\Omega_s,\gamma\}$ are {65, 47, 0.41Γ, 0.52Γ, 0.14Γ, 0.0022Γ}, respectively.

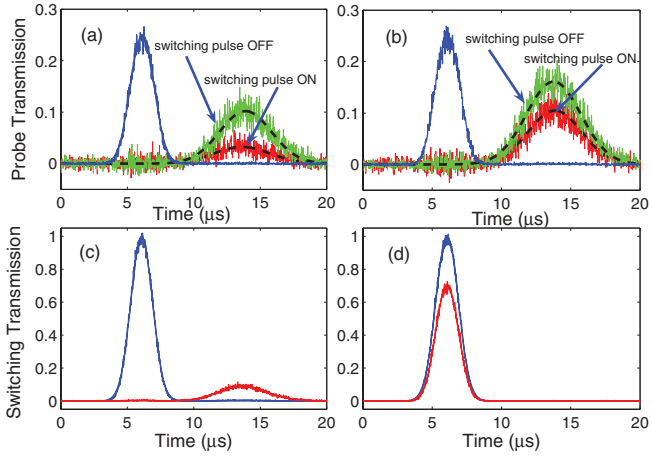

FIG. 3. (Color online) (a), (b) [(c), (d)] Probe (Switching) transmission versus time. The input probe (switching) pulses are also shown (blue). They are scaled down by 25% for clarity in (a) and (b). (a) and (c) were taken with the DSL scheme under a magnetic field of 1.9 G. (b) and (d) were taken with the N-type scheme. Gaussian fitting curves for the delayed probe pulses are shown in (a) and (b). The parameters $\{\alpha_p,\alpha_s,\Omega_{c1},\Omega_{c2}\}$ are {51, 77, 0.46Γ, 0.53Γ} for both cases. The delayed probe pulse with the switching off in (a) is a little weaker than that in (b). This is due to the off-resonant excitation of control 2 through the $|F = 4, m = 4\rangle \rightarrow |F' = 5, m = 5\rangle$ transition which degrades γ. In (d), the switching pulse for the N-type system is attenuated a little. Part of the attenuation (∼20%) is due to the imperfect optical pumping with a residual population in state $|6\rangle$. Another part (∼10%) is due to the nonlinear switching loss from the probe.

magnetic field. Both pulses have square waveforms with a duration of 20 μs. The input power of the probe and switching pulses are 2.0 and 13.5 nW, respectively. The output power of the two pulses during 12 to 20 μs are recorded. The transmission spectrum for the switching is shown in Fig. 2(c). This is a typical EIT spectrum for optically dense atomic samples. The ratio of the probe power with and without the presence of the switching (T_p) versus δ_s is shown in Fig. 2(a). Using our previous DSL scheme, we would choose δ_s at the values indicated by the dashed lines in Figs. 2(a) and 2(c). Given such detunings, the switching efficiency for the probe is maximized. However, the switching almost attenuates to zero after passing through the medium because it is two-photon detuned. Figures 2(b) and 2(d) show the probe and switching transmission spectra after applying a magnetic field of ∼1.9 G. The striking difference is that the switching can be operated at its EIT resonance, while the probe can be operated at its maximum switching point simultaneously. The AOS efficiency is significantly enhanced because the attenuation of the switching is greatly reduced by keeping at its EIT resonance. The enhancement in the AOS efficiency is typically around a factor of 5–7 compared to our previous DSL scheme. The solid lines in Figs. 2(a) and 2(b) indicate the plots obtained with Eq. (5). The simple model fits the data reasonably well. The slight deviation in the line shape and degree of switching may due to the over simplification in the susceptibilities.

Next, probe and switching pulses with a Gaussian waveform and a FWHM duration of 2μs are applied in the experiment. We apply a magnetic field and tune it to a magnitude such that the AOS effect is at its maximum. We tune the group velocities of the two pulses to matching conditions by adjusting the OD ratio among the probe and switching transitions as described in the previous section. Figures 3(a) and 3(c) show the typical data for DSL scheme. The energies of the probe and switching pulses are 5 and 55 fJ, respectively.

The ratio of the amplitude of delayed probe pulses with and without the presence of the switching pulses (T_p) characterizes the degree of nonlinear switching at the probe peak. A typical plot of T_p versus N_s for the DSL scheme is shown in the red circle trace of Fig. 4(a). Equation (6) describes T_p at a fixed switching intensity. To quantitatively fit the data for T_p versus N_s, we have to consider the Gaussian intensity distribution of the laser beams and perform the transverse averaging. With such a consideration, we obtain $T_p = \frac{1-\exp[\psi(N_s/A)\sigma_s]}{\psi(N_s/A)\sigma_s}$ [24].

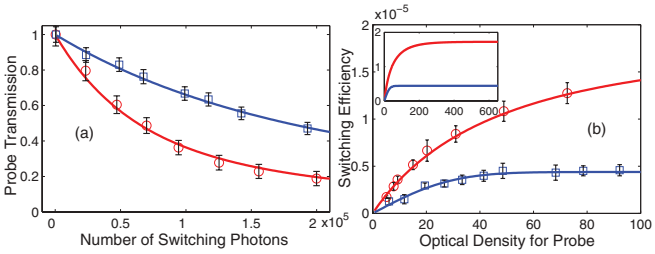

FIG. 4. (Color online) (a) T_p versus N_s for the DSL (red circles) and N-type (blue squares) schemes. The parameters $\{\alpha_p, \alpha_s, \Omega_{c1}, \Omega_{c2}\}$ are {73, 81, 0.54Γ, 0.60Γ} for the DSL scheme. The parameters $\{\alpha_p, \Omega_{c1}\}$ are {79, 0.54Γ} for the N-type scheme. (b) $1/N_0$ versus α_p for both the DSL (red circle) and N-type (blue square) schemes. The solid lines are the theoretical curves using Eqs. (7) and (9). The parameters $\{\Omega_{c1}, \Omega_{c2}, \gamma\}$ are {0.55Γ, 0.55Γ, 0.0012Γ} for the DSL scheme. The parameters $\{\Omega_{c1}, \tau_s\}$ are {0.93Γ, 2μs} for the N-type scheme.

We fit T_p versus N_s to the relation $T_p = \frac{1-e^{-N_s/N_0}}{N_s/N_0}$, where $N_0 = \frac{A}{\psi\sigma_s}$. The fits to the data are very good as shown by the solid lines in Fig. 4(a). Although we can determine the absolute efficiency ψ by knowing the beam waist ($\sim 50\mu m$), we also perform the same measurements for the N-type system formed by states $|1\rangle$ to $|4\rangle$ and do a relative comparison in ψ to avoid possible systematic problem. The ratio of $1/N_0$ for the two schemes reflects their efficiency ratio.

In the N-type experiment, we turn off control 2 and optically pump the population to state $|1\rangle$. There is a complication related to the AOS in our N-type system due to the possibility of forming four-wave mixing because the transition from state $|4\rangle$ to $|1\rangle$ is allowed. According to Ref. [25], the N-type switching results can be retained as if the transition from state $|4\rangle$ to $|1\rangle$ is forbidden if one operates the switching at an optimum detuning determined by the ODs and geometry. We take the N-type data at the optimum δ_s for each OD. Typical data for the N-type system are shown in Figs. 3(b) and 3(d). The experimental parameters are the same as those in the DSL scheme. Comparing the two traces with and without switching pulses in Figs. 3(a) and 3(b), it is clear that the switching efficiency for the DSL scheme is better than that of the N-type scheme.

We then systematically measure $1/N_0$ versus α_p in both schemes as shown in Fig. 4(b). In the DSL scheme, we keep $\alpha_p \simeq \alpha_s$. The nonlinear efficiency for the N-type scheme saturates to a maximum value at $\alpha_p \sim 50$. This behavior is expected and is due to the group velocity mismatch [4]. However, the nonlinear efficiency for the DSL scheme is still increasing around this range of α_p. At the highest OD, we have achieved an enhancement in the AOS efficiency by a factor of 3 compared to that of N-type scheme. The theoretical curve for the N-type scheme based on Eq. (7) is shown as the blue solid line in Fig. 4(b) with a scaling factor representing σ_s/A. The theoretical maximum value of ψ for the N-type scheme is 0.5 [4]. From Eq. (6), this corresponds to active an attenuation of probe to e^{-1} by two photons per atomic cross section. Our best switching efficiency with DSL scheme is thus 0.67 photons per atomic cross section. The solid red line in Fig. 4(b) indicates the plot for the DSL scheme obtained by Eq. (9) with the same scaling factor σ_s/A. At very high OD ($\sim$300), the theoretical prediction shows that the efficiency for the DSL scheme also approaches to a saturated value as shown in the inset to Fig. 4(b) due to finite γ and pulse broadening. Reducing γ, achieving a higher OD and operating at a higher Ω_c help to maximize ψ. As mentioned in Sec. II, the AOS efficiency ψ based on the DSL scheme has a square root scaling law versus OD. The AOS scheme using the stored and stationary light has a linear scaling law for ψ versus OD [22]. This scheme has been demonstrated recently, which obtained a maximum enhancement of 3.6 over the N-type limit [24].

V. CONCLUSION

In conclusion, we have demonstrated an improved DSL and AOS scheme, which allows both EIT systems on their two-photon resonances but with nonzero cross-Kerr nonlinearities. Based on this scheme, we have overcome the N-type switching limit by a factor of 3. Better nonlinear efficiency can be obtained if higher ODs could be achieved. If focusing the beams to the level of atomic cross section, our work implies that it is feasible to have significant efficiency for nonlinear optical processes at the single-photon level. Our work also provides essential ingredients to study the many-body physics utilizing strongly interacting photons.

ACKNOWLEDGMENTS

This work was supported by the National Science Council of Taiwan under NSC Grants No. 97-2112-M-028-MY3, No. 99-2628-M-001-021, and No. 100-2628-M-001-001. I.A.Y. acknowledges FP7 COLIMA (Project No. 247475).

APPENDIX: NUMERICAL CALCULATION OF THE SUSCEPTIBILITIES

We will present in this appendix the results of numerical calculation of the optical Bloch equation for the ten-level system shown in Fig. 1(a) with the presence of a magnetic field. From the results we show that the overall atomic responses from ρ_{21} and ρ_{98} resemble the results from a five-level M-type system (M_1) only. An explanation of why this is the case and under what parameter domains this approximation is valid is given.

Before discussing the ten-level system, we first consider the atomic response for the probe transition from ρ_{21} or ρ_{98} in a simple five-level M-type system like M_1 or M_2. In the actual energy level of cesium atoms, the population for each excited state in one specific M-type system has the possibility to spontaneously decay to the ground state of the other M-type system. To model the simple five-level system as a closed system, we scale up the spontaneous decay rate from the excited state to the ground state belonging to the same M-type system such that the total spontaneous decay rate of the excited state within the same M-type system is Γ. The analytic solution for steady-state density matrix elements ρ_{21} or ρ_{98} in a simple five-level system can be derived using the perturbation theory. The susceptibility is proportional to the density matrix element. The explicit expression for the cross-Kerr susceptibility $\chi_{21}^{(3,ck)}$ is shown in Eq. (2) while $\chi_{98}^{(3,ck)}$ can be referred to Supplemental Material of Ref. 10. To be more general to all possible magnitudes for the parameters, we perform an exact numerical calculation for the simple five-level system like the M_1 or M_2. We do not assume the presence of Zeeman shifts in this calculation. However, we can assume suitable detuning for each transition to model the five-level system under the presence of a magnetic field. For the M_1 system, the two transitions for the right Λ section are assumed to be at their one-photon resonances. The right Λ section in M_1 is thus at its two-photon resonance. Under such a condition, the linear susceptibility ($\chi^{(1)}$) is a constant value or zero if we assume the ground-state decoherence rate γ to be zero. For the simplicity of analysis, we assume that γ is zero in the numerical calculation so that the probe susceptibility is purely due to the cross-Kerr effect. The detunings of control 2, control 1, and the probe with respect to the $|5\rangle \rightarrow |4\rangle$, $|10\rangle \rightarrow |9\rangle$, and $|8\rangle \rightarrow |9\rangle$ transition are 0.0085 Γ, $-0.127\ \Gamma$, and $0.127\ \Gamma$, respectively. These detunings are the corresponding values when we keep the control 2, control

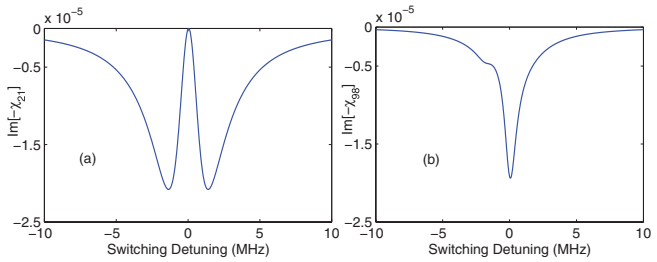

FIG. 5. (Color online) (a), (b) The steady-state calculation of $\mathrm{Im}[-\chi_{21}]$ and $\mathrm{Im}[-\chi_{98}]$ for the simple five-level M-type system M_1 and M_2, respectively. The Rabi frequencies Ω_{c1}, Ω_{c2}, Ω_p, and Ω_s with respect to $|3\rangle \rightarrow |2\rangle$, $|8\rangle \rightarrow |7\rangle$, $|1\rangle \rightarrow |2\rangle$ and $|6\rangle \rightarrow |7\rangle$ are 0.40 Γ, 0.40 Γ, 0.012 Γ, and 0.094 Γ, respectively. The detunings for each transition and the spontaneous decay rates for each excited state have been described in the context. We assume that γ is zero and atom density is $6 \times 10^{10}\mathrm{cm}^{-3}$.

1, and the probe at their one-photon resonances with respect to the $|8\rangle \rightarrow |7\rangle$, $|3\rangle \rightarrow |2\rangle$, and $|1\rangle \rightarrow |2\rangle$ transition in the presence of a magnetic field of 1.9 G. In the M_2 system, the detuning for switching with respect to transition $|6\rangle \rightarrow |7\rangle$ is scanned. Figures 5(a) and 5(b) show the imaginary part of the cross-Kerr susceptibilities for χ_{21} and χ_{98} in the generic five-level systems M_1 and M_2. The line shape of $\mathrm{Im}(-\chi_{21})$ for the M_1 system is a typical dispersive profile for the asymmetric five-level M-type system. The spacing of the two absorption peaks is equal to the Rabi frequency of the control field with respect to transition $|5\rangle \rightarrow |4\rangle$. The line shape of $\mathrm{Im}(-\chi_{98})$ in the M_2 system shows a narrow feature plus a broad feature. The narrow feature is centered at the condition when the switching field is scanned to the resonance of the $|6\rangle \rightarrow |7\rangle$ transition. This can be understood as a multiphoton transition with a pathway from $|6\rangle \rightarrow |7\rangle \rightarrow |8\rangle \rightarrow |9\rangle$. The broad feature is due to the one-photon absorption through $|8\rangle \rightarrow |9\rangle$ with a small population being optically pumped to state $|8\rangle$ by the switching field.

Next, we consider the numerical calculation for the ten-level system with Zeeman shifts as shown in Fig. 1(a). We perform both the steady-state and transient calculations. The Rung-Kutta method is used for the transient calculations. All atomic parameters are used according to the actual cesium data. The only exception is the spontaneous decay rate from state $|9\rangle \rightarrow |5\rangle$. The ten-level system considered here is actually incomplete because there are more Zeeman sublevels involved. However, the simplification with only a ten-level system is reasonable if we consider the cross-Kerr effect only to the third-order susceptibility. There is a possibility that the population may leave the ten-level system (e.g., spontaneous decay from state $|9\rangle$ to ground state $|F = 4, m = 1\rangle$). We artificially attribute the total spontaneous emission rate from state $|9\rangle$ out of the ten-level system ($\frac{\Gamma}{48}$) to the state $|5\rangle$ to ensure the conservation of population inside the ten-level system. This rate is small and its effect is expected to be small in the pulsed experiments. Typical steady-state calculations for the susceptibilities $\mathrm{Im}(-\chi_{21})$ and $\mathrm{Im}(-\chi_{98})$ are shown in Figs. 6(a)

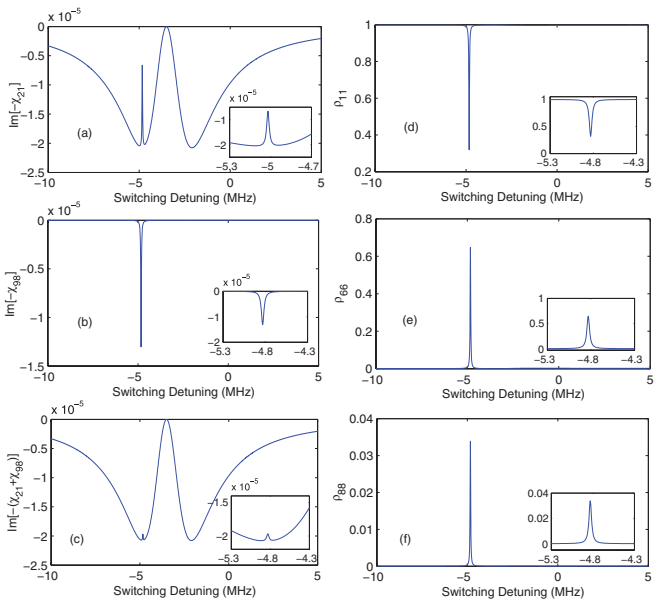

FIG. 6. (Color online) (a), (b), (c) The steady-state calculation of $\mathrm{Im}[-\chi_{21}]$, $\mathrm{Im}[-\chi_{98}]$ and $\mathrm{Im}[-(\chi_{21} + \chi_{98})]$ for the ten-level system in the presence of a magnetic field of 1.9 G. The Rabi frequencies for each transition are the same as those in Fig. 5. (d), (e), and (f) depict the population in states $|1\rangle$, $|6\rangle$ and $|8\rangle$, respectively. The insets show an enlargement of the narrow feature when the switching field is scanned through the resonance with respect to the $|6\rangle \rightarrow |7\rangle$ transition.

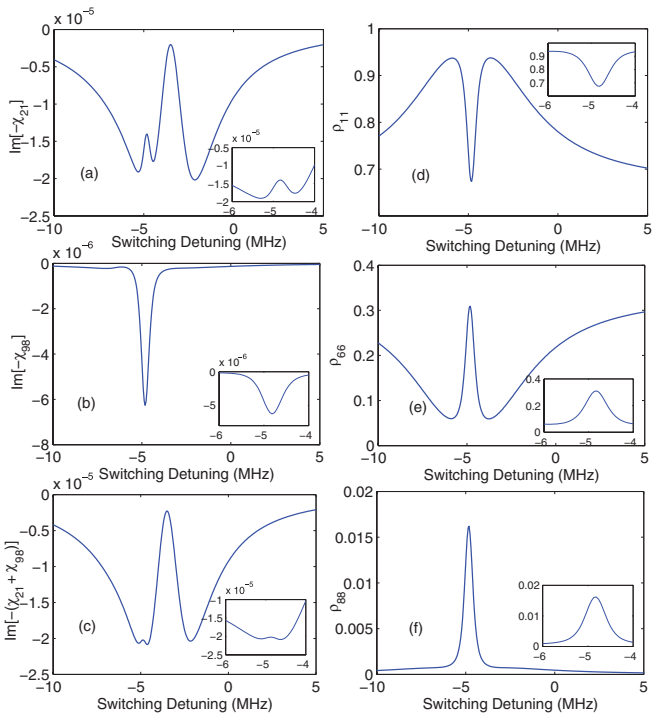

FIG. 7. (Color online) (a), (b), (c) The transient calculation of $\mathrm{Im}[-\chi_{21}]$, $\mathrm{Im}[-\chi_{98}]$ and $\mathrm{Im}[-(\chi_{21} + \chi_{98})]$ for the ten-level system under the presence of a magnetic field of 1.9 G. The Rabi frequencies for each transition are the same as those for Fig. 5. (d), (e), and (f) depict the population in states $|1\rangle$, $|6\rangle$ and $|8\rangle$, respectively. The evolution time is $400/\Gamma$. The insets show an enlargement of the narrow feature when the switching field is scanned through the resonance with respect to the $|6\rangle \rightarrow |7\rangle$ transition.

and 6(b) with the presence of a magnetic field of 1.9 G. The profile for the $\mathrm{Im}(-\chi_{98})$ in the ten-level system is very similar to that in the five-level M_2 system but with a narrower line width. The general profile for the $\mathrm{Im}(-\chi_{21})$ in the ten-level system is very similar to that in the five-level M_1 system, except that there is a narrow peak feature, which appears when the switching field is scanned through resonance of the $|6\rangle \rightarrow |7\rangle$ transition. The explanation for this additional peak feature is related to the population exchange between states $|1\rangle$ and $|6\rangle$ in the two M-type systems. Figures 6(d)–6(f) show the population of states $|1\rangle$, $|6\rangle$ and $|8\rangle$ at the steady state. In the steady-state calculation, the population will be optically pumped out of state $|6\rangle$ by the switching field if it is off-resonant with respect to the $|6\rangle \rightarrow |7\rangle$ transition. Due to the optical pumping effect of the control 2, all populations will be almost completely in state $|1\rangle$ in the long time limit. The probe absorption through transition $|8\rangle \rightarrow |9\rangle$ is thus almost zero for the off-resonant switching field, because there is no population in state $|8\rangle$ for direct one-photon transition and there is no population in state $|6\rangle$ for multiphoton transition through the pathway $|6\rangle \rightarrow |7\rangle \rightarrow |8\rangle \rightarrow |9\rangle$. The probe absorption through transition $|1\rangle \rightarrow |2\rangle$ is almost the same as for a simple five-level M_1 system for the off-resonant switching field because all population are almost in state $|1\rangle$ under such conditions. If the switching field is on resonance of transition $|6\rangle \rightarrow |7\rangle$, the population in state $|6\rangle$ will stay in the same state due to the protection of the switching's EIT dark resonance. Thus, the probe absorption through transition $|8\rangle \rightarrow |9\rangle$ occurs for an on-resonant switching field through one-photon transition from state $|8\rangle$ and through multiphoton transition through the pathway $|6\rangle \rightarrow |7\rangle \rightarrow |8\rangle \rightarrow |9\rangle$. The multiphoton absorption dominates because the population in state $|6\rangle$ is much larger than that in state $|8\rangle$. Due to the population dip in state $|1\rangle$, the probe absorption through $|1\rangle \rightarrow |2\rangle$ has a peak for on-resonant switching field. The contribution of the narrow features from $\mathrm{Im}(-\chi_{21})$ and $\mathrm{Im}(-\chi_{98})$ in the ten-level system almost cancel each other and the overall profile is thus very similar to the profile of $\mathrm{Im}(-\chi_{21})$ of a simple five-level system like M_1. The degree of cancellation of the narrow features depends mostly on the magnitudes of the Rabi frequency of the control fields. With $\Omega_{c1,32} \simeq \Omega_{c2,87}$, the cancellation is nearly perfect. If $\Omega_{c1,32} > (<)\Omega_{c2,87}$, the absolute magnitude of the narrow feature due to $\mathrm{Im}(-\chi_{21})$ is larger (smaller) than that due to $\mathrm{Im}(-\chi_{98})$. In the experiments, we keep $\Omega_{c1,32} \simeq \Omega_{c2,87}$ for the group velocity matching condition, and thus the probe response by a simple five-level M_1 system is a good approximation to that for a ten-level system. We have checked that the cancellation of the two narrow features is good to 15% if the difference in the two Rabi frequencies for control fields are within $\pm 10\%$. The Rabi frequencies of the probe and switching fields affect the line width of the narrow features but there is no significant change in the degree of cancellation.

The transient calculations with an evolution time of $400/\Gamma$ are shown in Fig. 7. The qualitative behavior is similar to the steady-state calculation except that the line width of the narrow features is wider and the degree of population exchange is not as large as that in the steady state. The degree of cancellation in the narrow features is, however, similar to that of the steady-state results. The conclusion that the overall probe absorption for the ten-level system can be approximately modeled by that of a simple five-level system like M_1 in the suitable parameter domain also holds for the pulsed experiments.

[1] For a recent review, see, e.g., M. Fleischhauer, A. Imamoğlu, and J. P. Marangos, Rev. Mod. Phys. **77**, 633 (2005).

[2] H. Schmidt and A. Imamoğlu, Opt. Lett. **21**, 1936 (1996).

[3] S. E. Harris and Y. Yamamoto, Phys. Rev. Lett. **81**, 3611 (1998).

[4] S. E. Harris and L. V. Hau, Phys. Rev. Lett. **82**, 4611 (1999).

[5] M. D. Lukin and A. Imamoğlu, Phys. Rev. Lett. **84**, 1419 (2000).

[6] D. Petrosyan and Gershon Kurizki, Phys. Rev. A **65**, 033833 (2002).

[7] S. Rebić, D. Vitali, C. Ottaviani, P. Tombesi, M. Artoni, F. Cataliotti, and R. Corbalán, Phys. Rev. A **70**, 032317 (2004).

[8] D. Petrosyan and Y. P. Malakyan, Phys. Rev. A **70**, 023822 (2004).

[9] Z.-B. Wang, K.-P. Marzlin, and B. C. Sanders, Phys. Rev. Lett. **97**, 063901 (2006).

[10] B.-W. Shiau, M.-C. Wu, C.-C. Lin, and Y.-C. Chen, Phys. Rev. Lett. **106**, 193006 (2011).

[11] C. Ottaviani, D. Vitali, M. Artoni, F. Cataliotti, and P. Tombesi, Phys. Rev. Lett. **90**, 197902 (2003).

[12] C. Ottaviani, S. Rebić, D. Vitali, and P. Tombesi, Eur. Phys. J. D **40**, 281 (2006).

[13] D. A. Braje, V. Balić, G. Y. Yin, and S. E. Harris, Phys. Rev. A **68**, 041801(R) (2003).

[14] Y.-F. Chen, Z.-H. Tsai, Y.-C. Liu, and I. A. Yu, Opt. Lett. **30**, 3207 (2005).

[15] M. Bajcsy, S. Hofferberth, V. Balic, T. Peyronel, M. Hafezi, A. S. Zibrov, V. Vuletić, and M. D. Lukin, Phys. Rev. Lett. **102**, 203902 (2009).

[16] D. E. Chang, V. Gritsev, G. Morigi, V. Vultetic, M. D. Lukinm, and E. A. Demler, Nature Phys. **4**, 884 (2008).

[17] M. Kiffner and M. J. Hartmann, Phys. Rev. A **81**, 021806(R) (2010).

[18] D. G. Angelakis, M. Huo, E. Kyoseva, and L. C. Kwek, Phys. Rev. Lett. **106**, 153601 (2011).

[19] M. A. Antón, F. Carreño, O. G. Calderón, S. Melle, and I. Gonzalo, Opt. Commun. **281**, 6040 (2008).

[20] P. Lambropoulos and D. Petrosyan, *Fundamentals of Quantum Optics and Quantum Information* (Springer, Berlin, 2006), Chap. 6.

[21] Y.-F. Chen, Y.-M. Kao, W.-H. Lin, and Ite A. Yu, Phys. Rev. A **74**, 063807 (2006).

[22] A. André, M. Bajcsy, A. S. Zibrov, and M. D. Lukin, Phys. Rev. Lett. **94**, 063902 (2005).

[23] Y.-W. Lin, H.-C. Chou, P. P. Dwivedi, Y.-C. Chen, and I. A. Yu, Opt. Express. **16**, 3753 (2008).

[24] Y.-H. Chen, M.-J. Lee, W. Hung, Y.-C. Chen, Y.-F. Chen, and I. A. Yu, Phys. Rev. Lett. **108**, 173603 (2012).

[25] M.-J. Lee, Y.-H. Chen, I-C. Wang and Ite A. Yu, Opt. Express **20**, 11057 (2012).